geosciences

MDPI

Article

Assessing the Influence Zone and Drainage Efficiency of Geotextiles with Enhanced Lateral Drainage Abilities in Unsaturated Soil Systems

Shakeel Abid Mohammed * and Jorge G. Zornberg *

Department of Civil, Architectural and Environmental Engineering, The University of Texas at Austin, 301 E. Dean Keeton St., Austin, TX 78712, USA

* Correspondence: mdshakeelabid@gmail.com (S.A.M.); zornberg@mail.utexas.edu (J.G.Z.)

Abstract

The hydraulic performance of woven geotextiles is frequently overlooked in roadway design, despite their extensive use for reinforcement applications. Woven geotextiles are typically manufactured from hydrophobic polymers such as polypropylene or polyester and can act as capillary barriers under unsaturated conditions. This results in moisture accumulation at the soil–geotextile interface, adversely impacting long-term pavement performance. Such problems can be effectively mitigated using geotextiles with enhanced lateral drainage (ELD) capabilities, which are engineered with hydrophilic fibers to facilitate capillary-driven lateral water movement under unsaturated conditions. This functionality facilitates the redistribution of moisture away from the interface, mitigating moisture retention and enhancing drainage performance. The hydraulic performance of geotextiles with enhanced lateral drainage capabilities under unsaturated conditions remains insufficiently understood, particularly in terms of their influence zone and drainage efficiency. For this reason, the present study evaluates the lateral drainage behavior of an ELD geotextile using a soil column test, compared against a control setup without a geotextile and with a non-woven geotextile. Two moisture migration scenarios, namely capillary rise and vertical infiltration, were simulated, with the water table varied at multiple depths. Moisture sensors were embedded along the column depth to monitor real-time water content variations. Results show that the ELD geotextile facilitated efficient lateral drainage, with a consistent influence zone extending up to 2 inches below the fabric. Under infiltration, the ELD geotextile reduced moisture accumulation by 30% around the geotextile, highlighting its superior drainage behavior. These findings encourage practicing engineers to adopt rational, performance-based designs that leverage ELD geotextiles to enhance subgrade drainage and moisture control in pavement and geotechnical applications.

Keywords: geotextiles; wicking; lateral drainage; hydraulic barrier

Academic Editors: Laureano R. Hoyos, Dunja Perić and Aritra Banerjee

Received: 31 October 2025
Revised: 15 December 2025
Accepted: 24 December 2025
Published: 1 January 2026

1. Introduction

Moisture-induced distress is widely recognized as one of the most significant factors affecting the long-term performance of pavements and embankments. The hydraulic state of the subgrade and base layers plays a pivotal role in governing the stress–strain response of pavement systems as matric suction, effective stress, and stiffness are highly sensitive to variations in moisture content, thereby influencing deformation characteristics and long-term structural performance [1–3]. Even small variations in water content can

cause disproportionate losses in mechanical integrity, for example, laboratory and field studies have reported up to 50% reductions in resilient modulus of granular bases when moisture contents rise by only a few percent above optimum [4–6]. Furthermore, under repeated traffic loading, excess water accelerates plastic deformation, fines migration, and fatigue cracking [7,8], while in cold climates, trapped water enhances frost heave and thaw weakening [9,10]. These combined effects lead to rutting, pumping, and premature cracking, resulting in escalating maintenance costs and shortened pavement service life [11,12].

Geosynthetics have become an integral component of modern pavement and embankment design, extensively used to mitigate performance issues associated with moisture variation [13]. They are routinely employed to perform multiple functions, including separation, filtration, reinforcement, and drainage [14,15] Their mechanical and filtration benefits, such as improved confinement, reduced fines migration, and increased bearing capacity, have been extensively validated through laboratory studies and full-scale field applications [16–18]. However, the hydraulic behavior of geosynthetics under unsaturated conditions, which are common during pavement service life, remains less explored [19,20]. Conventional non-woven geotextiles and drainage composites perform efficiently under saturated flow, where gravitational gradients dominate. In reality, pavement subgrades seldom achieve full saturation; instead, they experience transient moisture regimes driven by capillary and suction gradients [21,22]. In unsaturated systems, capillary barriers are developed at interfaces between two porous materials with contrasting hydraulic conductivities and pore-size distributions [23,24]. The finer medium retains water within its small pores, while flow into the coarser medium is inhibited until the matric suction decreases below a threshold value known as the breakthrough suction [25,26]. Geotextiles generally possess large pore openings and hydrophobic polymer surfaces; their hydraulic response resembles that of coarse-grained soils [27,28]. When installed beneath fine-grained subgrades, these fabrics can act as capillary breaks, temporarily impeding downward drainage and promoting moisture accumulation above the interface [29]. While such behavior can be advantageous in systems intentionally designed to retain moisture, such as evapotranspirative landfill covers or frost-protection layers [30,31], it is generally detrimental in pavement applications. Excess moisture trapped above the geotextile reduces matric suction and effective stress, leading to lower resilient modulus, increased plastic strain accumulation, and slower hydraulic recovery following rainfall or groundwater rise [32,33]. Over time, these conditions accelerate moisture-induced rutting, pumping, and differential settlement in the subgrade [5,13]. This highlights the necessity for hydraulically responsive geosynthetics that maintain capillary continuity and regulate suction-driven flow, thereby improving the long-term moisture stability and structural resilience of pavement systems operating under unsaturated conditions

Recent advancements in geosynthetic technology have aimed to overcome the hydraulic discontinuity induced by conventional non-woven fabrics. New enhanced lateral drainage (ELD) or wicking geotextiles have been specifically engineered to operate as capillary-active drainage layers capable of transporting water under both saturated and unsaturated conditions [34–38]. These fabrics incorporate hydrophilic, multi-channeled 4DG nylon fibers interwoven with polypropylene yarns, forming a hierarchical network of intra-pore grooves, inter-fiber contacts, and inter-yarn pathways that sustain continuous water films along longitudinal channels [39]. Under unsaturated conditions, the fine grooves generate high local capillary suction that draws water from adjacent soil pores into the fiber network, while the inter-yarn plane provides high in-plane flow for suction-driven lateral redistribution. This multiscale connectivity allows the fabric to absorb excess pore water and transmit it toward edge drains or shoulders, thereby dissipating moisture that would otherwise accumulate above/below the interface. Laboratory and field investigations have

reported reductions of 2–3% in equilibrium water content and corresponding twofold increases in resilient modulus for base layers incorporating wicking geotextiles [40,41]. Complementary numerical and coupled hydro-thermal analyses further demonstrate that these fabrics can reduce moisture accumulation by 25–30% and shorten recovery times after rainfall or water-table fluctuations by over 40% [42].

Despite these promising findings, the unsaturated hydraulic behavior of ELD geotextiles have not been extensively characterized. Fundamental uncertainties persist regarding the spatial extent of their influence zone, the efficiency of suction-driven drainage, and the stability of their capillary performance under cyclic wetting and drying [42,43]. In particular, the water balance, the dynamic interplay among inflow, storage, and outflow within a soil–geotextile composite, has seldom been quantified under controlled laboratory conditions [6,21]. Understanding these factors is essential for linking pore-scale capillary processes to field-scale hydraulic response, as the equilibrium between infiltration, redistribution, and drainage effects suction recovery and effective stress evolution in pavement subgrades [44]. Without such mechanistic insight, contemporary pavement design frameworks, including AASHTO (1993) [45] and the MEPDG (2008) [46], continue to treat drainage as a purely saturated process, neglecting the unsaturated flow regimes and suction-regulated moisture control provided by capillary-active geosynthetics.

The present study addresses these gaps through a systematic experimental investigation of the transient hydraulic response and water-balance behavior of soil–geotextile systems under controlled boundary conditions. A series of instrumented soil column experiments were conducted using a representative 20% kaolin–80% sand mixture to replicate subgrade hydraulic behavior. Each column was subjected sequentially to equilibrium, water-table rise, drainage, and infiltration stages to simulate field boundary fluctuations. Continuous monitoring of volumetric moisture content and matric suction allowed quantification of spatial and temporal variations in storage and moisture redistribution above and below the geotextile interface. Comparisons were made among a control column (no geotextile), a conventional non-woven polypropylene geotextile (Mirafi N140), and a wicking ELD geotextile (Mirafi H2Ri) to assess how fiber wettability and structure influence unsaturated hydraulic behavior. By integrating high-resolution sensor data with spatial contour visualization, this study quantifies the influence zone, storage variation, and drainage continuity of each geotextile type. These results provide new mechanistic insight into the unsaturated flow processes governing moisture redistribution in soil–geotextile systems.

2. Experimental Program and Test Setup

A systematic experimental program was designed to investigate the hydraulic response of non-woven and ELD geotextiles under transient groundwater and infiltration conditions representative of field subgrade conditions. The testing framework was developed to evaluate the variations in moisture storage, suction, and drainage characteristics of soil–geotextile systems subjected to different hydraulic boundary conditions, namely, (i) initial equilibrium with water table at 2 inches from bottom representing a baseline equilibrium with a steady phreatic surface, creating a stable capillary zone and suction profile representative of in situ conditions (maintained for 3 days) (ii) rise in water table by 1 inch representing a short-term groundwater rise after rainfall, generating an upward capillary movement through the unsaturated zone (2 days) (iii) drainage condition representing a receding groundwater table (1 day), and (iv) surface infiltration simulating a transient groundwater fluctuation during rainfall (2 days). These conditions are schematically illustrated in Figure 1. Each test was conducted for a total duration of nine days, including an additional one-day preconditioning period to achieve equilibrium prior to the

initial boundary condition. In addition to the geotextile tests, a control column without a geotextile was also tested under identical boundary conditions to isolate the effect of the geotextile on the overall hydraulic response. These sequential stages facilitated the characterization of water redistribution mechanisms in unsaturated soil columns and the assessment of the drainage efficiency of geotextiles (ratio of the water released during drainage to the total water stored at the onset of the drainage stage) with contrasting wetting properties.

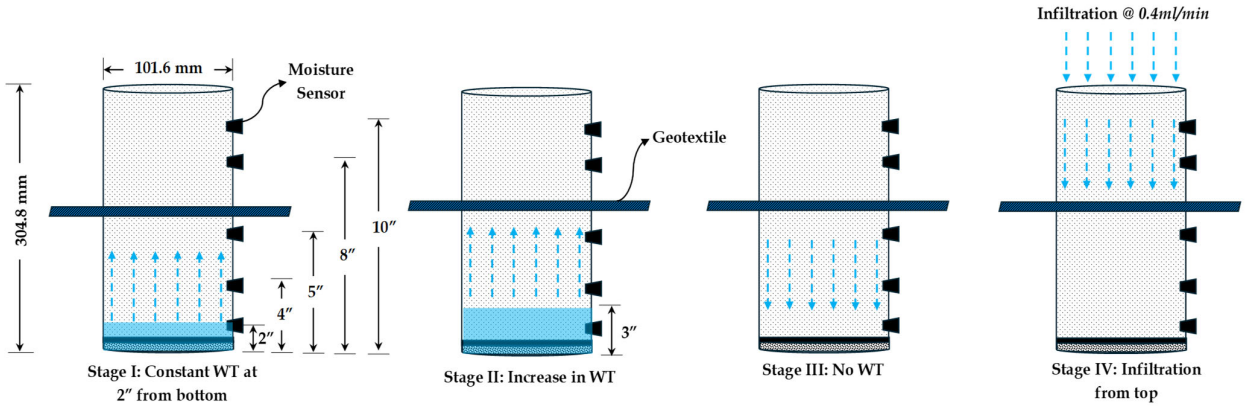

Figure 1. Schematic illustration of the test setup and testing program.

The experimental investigations were performed using a custom-built cylindrical soil column apparatus made of transparent acrylic to enable visual monitoring of wetting and drying fronts. The column had an internal diameter of 101.6 mm (4″) and a height of 304.8 mm (12″). The overall height was divided into two equal zones to simulate the soil layers above and below the geotextile interface. The base of the column assembly consisted of a coarse aggregate layer placed beneath a drainage geocomposite to ensure uniform inflow and outflow. Small perforations (5/64″) were provided in the lower acrylic section to permit controlled water exchange between the column and an external reservoir. The column was positioned within a constant-head reservoir, and the desired groundwater level within the soil column was maintained by adjusting the water level in this reservoir. An increase in the reservoir level induced a corresponding rise in the water table within the column, while drainage was simulated by lowering the reservoir level, allowing gravitational outflow through the base perforations and geocomposite layer. During the infiltration stage, a flow-controlled inflow system was employed using a peristaltic flow meter set at a rate of 0.4 mL/min to provide uniform infiltration from the top. A thin filter paper disc was placed on the surface to promote even moisture distribution and prevent localized ponding. This configuration ensured accurate control of hydraulic boundary conditions and realistic replication of field-scale water-table fluctuations and infiltration events within a one-dimensional soil column system. The geotextile was positioned at the mid-height of the column, corresponding to 150 mm from the base.

The soil was air-dried, pulverized, and sieved through a 2 mm sieve to ensure uniform gradation. The target dry unit weight of 15.5 kN/m^3, corresponding to a degree of compaction of approximately 90% of the Standard Proctor maximum, was achieved through controlled layer-wise compaction using a circular tamper. The soil was placed in five lifts of 60 mm thickness each to minimize density variations along the column height. Each column was allowed to equilibrate for 24 h before initiating the hydraulic boundary condition. A non-woven geotextile and an ELD geotextile were used and were cut into rectangular strips matching the column diameter and placed horizontally at mid-height, with 15 cm of the strip being extended beyond the column on both sides. The ELD geotextile was oriented such that the wicking yarns were aligned along the lateral direction to promote lateral

moisture migration under capillary gradients. Instrumentation in each column included five EC-5 soil moisture sensors (accuracy ± 0.002 m^3/m^3) installed at depths of 2″, 4″, 5″, 8″, and 10″ from the top. Calibration of the EC-5 sensors was performed using the same soil mixture adopted in the experiments to ensure accurate measurement of volumetric water content. The calibration included repeated wetting and drying cycles to reduce hysteresis effects and confirm consistent sensor response across the expected moisture range. A ZL6 data logger manufactured by Meter Group was used which continuously recorded the volumetric moisture content during all hydraulic stages. The temporal evolution of water content was subsequently used to compute storage and drainage quantities using the water-balance approach.

Each test began by establishing the initial equilibrium water table condition at 2″ above the base. Once steady-state readings were achieved, the water table was raised by 1″. In the drainage stage, the free drainage was allowed, while moisture gradients were recorded until near equilibrium. The infiltration stage was initiated by uniformly applying a known volume of water (0.4 mL/min) at the column surface. All tests were conducted at room temperature (22 ± 2 °C). The column arrangement provided a one-dimensional vertical flow regime while allowing lateral drainage along the geotextile plane. The configuration ensured that differences in suction and moisture distribution could be attributed solely to the hydraulic characteristics of the geotextiles. The adopted setup thereby provided a reliable framework to quantify the influence of geotextile type, water-table fluctuation, and infiltration conditions on transient water storage and drainage efficiency in unsaturated soil systems. However, some uncertainty remains due to sensor resolution, local soil–sensor contact, and minor variability in compaction and boundary control. In addition, the one-dimensional column configuration represents an idealized condition and does not capture three-dimensional flow or stress states present in field pavements.

2.1. Geotechnical Properties of Soil and Geotextiles

2.1.1. Soil

The test soil comprised a mixture of 20% kaolin and 80% uniformly graded sand by dry weight, proportioned to replicate a subgrade soil with moderate plasticity and intermediate drainage capacity. The sand fraction provided the structural skeleton and governed permeability, while the kaolin fraction introduced slight cohesion and moisture retention. The mixture was air-dried, blended thoroughly, and compacted to a relative compaction of 90% corresponding to the target field density. The initial moisture content during placement was 7%, which ensured uniform compaction and minimized segregation during sample preparation.

The grain size distribution curve for the soil mixture is presented in Figure 2a. Approximately 21% of the particles were finer than 0.075 mm, and all particles passed the 2 mm sieve. Based on the Unified Soil Classification System (USCS), the material is classified as a clayey sand (SC), reflecting a predominantly sandy matrix containing plastic fines from kaolin. The other geotechnical properties of the soil are shown in Table 1. The soil–water retention curve (SWRC) for the 20% kaolin–80% sand mixture was determined using a combination of the hanging column, pressure plate, and dew-point potentiometer methods to cover a wide suction range. Measured data were fitted using the van Genuchten bimodal model [47,48]), which captured the distinct macro- and micro-pore drainage behavior characteristic of the sand–kaolin mixture. The SWRC of the soil, along with the fitting parameters are shown in Figure 2b. The air-entry value (AEV) for the macroporous domain was approximately 2 kPa, while the kaolin-dominated microporous domain exhibited an AEV near 1000 kPa, confirming two distinct drainage mechanisms. The saturated volumetric water content (θ_s) and residual water content (θ_r) were determined as 0.373 and 0.0149,

respectively. The curve exhibits a pronounced transition zone between approximately 10 and 1000 kPa, representing the shift from rapid macropore drainage to slow water release from micropores.

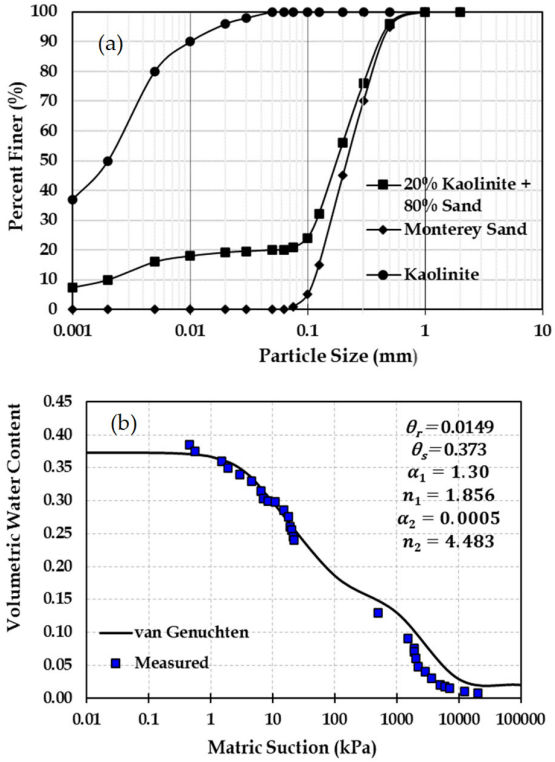

Figure 2. (**a**) Grain size distribution curve of 20% kaolin and 80% Monterey sand (**b**) SWRC of the soil mixture with 20% kaolin and 80% Monterey sand.

Table 1. Properties of 20% kaolin–80% sand mixture.

Parameters	Value
Specific gravity, G	2.60
Maximum dry unit weight, $\gamma_{d(max)}$, kN/m^3	17
Optimum moisture content (%)	10.80
Dry unit weight corresponding to 90% of standard proctor maximum, (kN/m^3)	15.50
Liquid Limit (%)	23
Plastic Limit (%)	18
Plasticity Index (%)	5

2.1.2. Geotextiles

A non-woven polypropylene geotextile (Mirafi N140) and an ELD geotextile (Mirafi H2Ri) designed to promote capillary-driven lateral flow under unsaturated conditions were used for the experimental studies (Figure 3a). The Mirafi N140 is a needle-punched, thermally bonded non-woven geotextile composed of hydrophobic polypropylene fibers. It is primarily used as a separator in pavement systems and conforms to AASHTO M288 Class 3 specifications. The material possesses a mass per unit area of 135 g/m^2, thickness of 0.9 mm, and apparent opening size (AOS) of 0.21 mm. The permittivity and flow were reported as 1.8 s^{-1} and 4 $\times$ 10^{-6} m^2/s, respectively. The fibers are randomly oriented, providing high permeability under saturated flow but exhibiting limited wetting under unsaturated conditions due to a contact angle exceeding 90°. Consequently, Mirafi N140 tends to act as a capillary barrier, impeding upward flow and causing localized moisture

accumulation at the soil–geotextile interface. This behavior is critical for assessing how conventional non-woven materials respond to transient hydraulic loading in unsaturated soil systems.

The Mirafi H2Ri is a woven fabric composed of polypropylene and nylon fibers. Its structure integrates grooved 4DG nylon fibers developed by Fiber Innovation Technology, Inc. (F.I.T.), which have deep longitudinal grooves (~8 µm) that provide continuous capillary channels for lateral moisture transport. Each yarn consists of approximately 150 wicking fibers bundled into strands, producing a hydrophilic and hygroscopic matrix capable of drawing water from the surrounding soil and redistributing it along the geotextile plane Figure 3b. The Mirafi H2Ri replaces part of the transverse polypropylene fibers with these nylon strands, resulting in a denser fabric that combines reinforcement and drainage functions. Manufacturer-reported properties include a thickness of 1.65 mm, mass per unit area of 575 g/m^2, AOS of 0.43 mm, permittivity of 0.4 s^{-1}, and a cross-plane hydraulic conductivity of 7 $\times$ 10^{-2} cm/s. The nylon fibers' strong capillary affinity, with a limited contact angle enables wicking-driven lateral flow, significantly reducing moisture storage above the interface compared with conventional non-woven materials. This wicking mechanism allows the ELD geotextile to redistribute moisture horizontally, thereby reducing moisture concentration and storage above the interface and enhancing overall drainage efficiency during wetting–drying cycles.

Scanning electron microscopic (SEM) tests were conducted to visualize 4DG fibers in ELD geotextiles and the images of both geotextiles are shown in Figure 3. The non-woven Mirafi N140 displays a randomly entangled network of polypropylene filaments with large, irregular pores, confirming its low surface roughness and limited wetting potential. In contrast, the wicking geotextile exhibits longitudinally aligned yarn bundles composed of grooved 4DG nylon fibers, which were clearly identified in the SEM images. The presence of these 4DG fibers was confirmed through SEM analysis, verifying their distinct grooved geometry that enables capillary-driven lateral drainage Figure 3c. These structural differences observed microscopically directly explain the contrasting moisture redistribution behaviors of the two geotextiles under fluctuating hydraulic conditions.

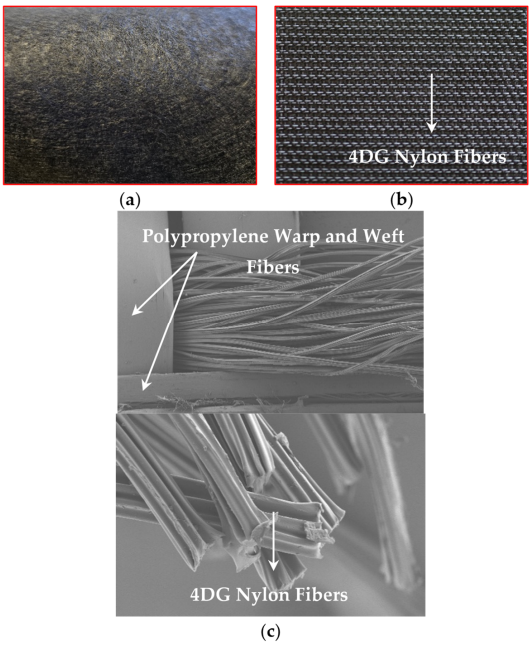

Figure 3. Geotextiles used for the study: (**a**) Mirafi N140 geotextile, (**b**) Mirafi H2Ri, (**c**) Microscopic view of Mirafi H2Ri.

3. Results and Discussions

3.1. Transient Moisture Variation and Drainage Mechanisms in Soil Columns with Non-Woven and Wicking Geotextiles

The variation of volumetric moisture content with time for the control column, the column with the non-woven geotextile, and the column with the ELD geotextile is presented in Figures 4–6. Furthermore, the contour plots of volumetric moisture distribution were generated from the measured time-series data using interpolated sensor readings throughout each hydraulic stage. The volumetric water content values obtained at different depths and discrete time intervals were processed using bilinear interpolation to estimate intermediate values across the entire 30 cm column domain. The resulting matrix was then contoured using a uniform color scale to represent the spatial and temporal evolution of moisture within the column. The upper and lower boundary conditions corresponded to the saturated and the dry surface, respectively. Each contour band thus represents a line of equal volumetric water content (θ), enabling visualization of the advancing and receding wetting fronts with time. The corresponding contour plots of volumetric moisture distribution with time and depth are shown in Figures 7–9. Together, these datasets provide a complete characterization of the transient hydraulic behavior of the soil–geotextile systems under sequential changes in boundary conditions. The time-series plots describe the dynamic evolution of volumetric moisture content at discrete depths, whereas the contour plots capture the spatial redistribution of wetting and drying fronts across the column. The combined interpretation of these data offers a mechanistic understanding of how geotextiles influence capillary continuity, water storage, and drainage efficiency within unsaturated soil profiles. These responses are representative of field subgrade environments, where seasonal fluctuations in groundwater table, infiltration, and evaporation cycles govern the hydraulic stability and long-term performance of pavement systems.

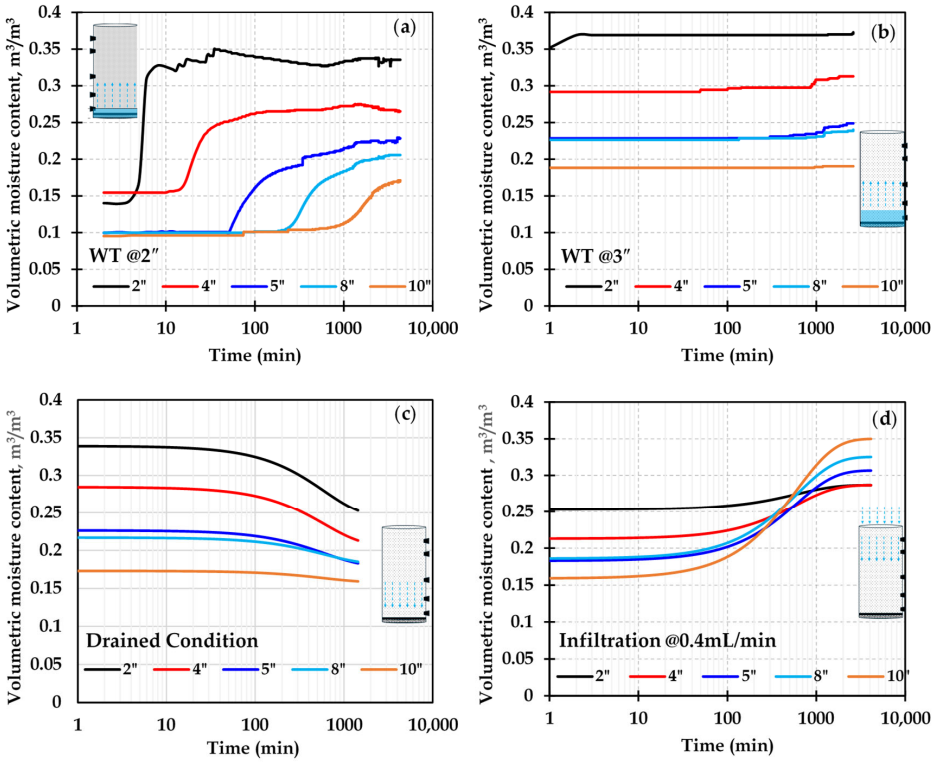

Figure 4. Variation in moisture content with time for the control column along different stages: (**a**) water table at 2″ from base, (**b**) water table at 3″ from base, (**c**) drained condition, (**d**) infiltration at the rate of 0.4 mL/min.

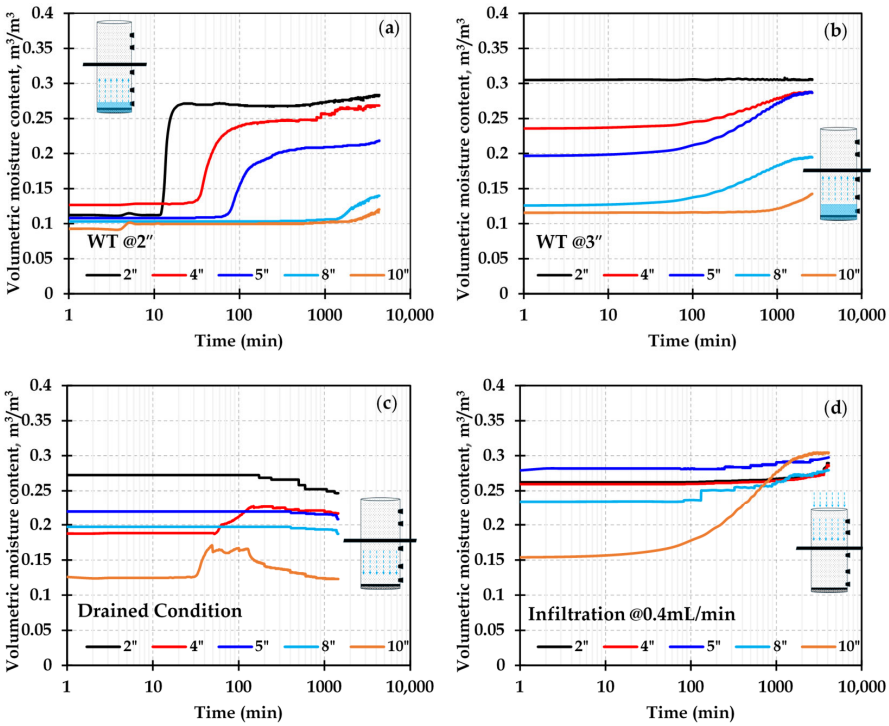

Figure 5. Variation in moisture content with time for the column with a non-woven geotextile along different stages: (**a**) water table at 2″ from base, (**b**) water table at 3″ from base, (**c**) drained condition, (**d**) infiltration at the rate of 0.4 mL/min.

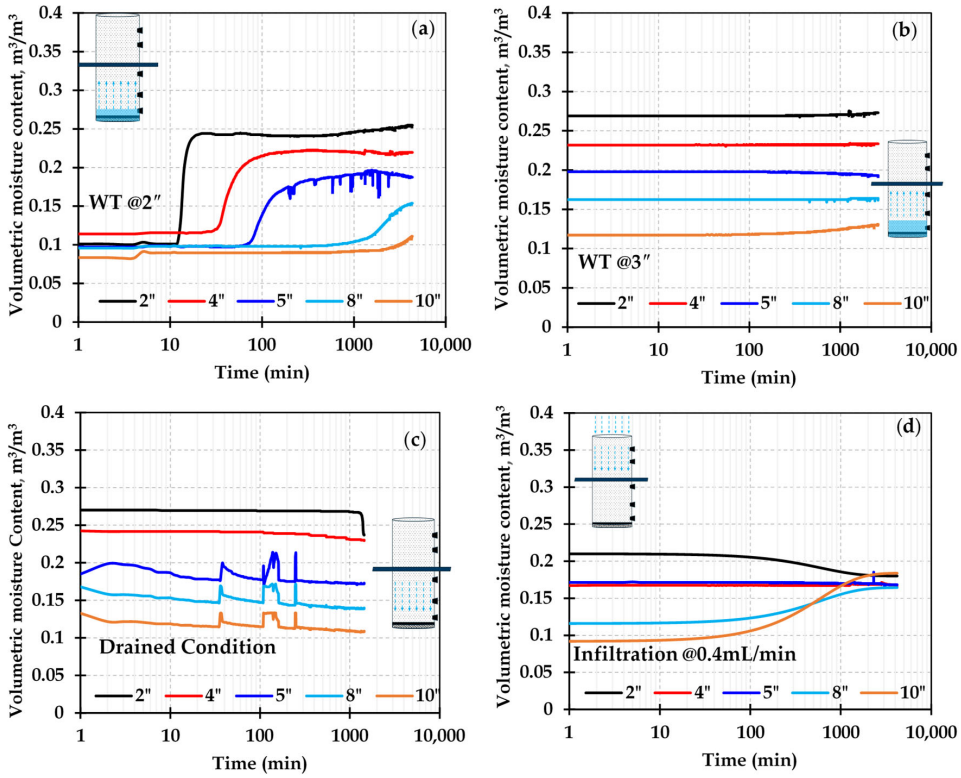

Figure 6. Variation in moisture content with time for the column with an ELD geotextile along different stages: (**a**) water table at 2″ from base, (**b**) water table at 3″ from base, (**c**) drained condition, (**d**) infiltration at the rate of 0.4 mL/min.

During the initial equilibrium stage with the water table at 2″, the control column exhibited a stable capillary rise profile consistent with the suction range typically ob-

served in lightly compacted fine-grained subgrades under shallow groundwater conditions (Figure 4a). The volumetric moisture content varied gradually from approximately 0.35–0.36 near the base to 0.16 near the surface, producing a smooth moisture gradient indicative of continuous liquid-phase connectivity. The corresponding contours (Figure 7a) showed evenly spaced color bands, confirming uniform capillary rise and the absence of hydraulic impedance. Such a profile replicates field conditions following extended dry periods, where capillary rise from a shallow water table gradually restores subgrade moisture to equilibrium levels. In contrast, the column with the non-woven geotextile displayed a clear discontinuity in the moisture profile near the geotextile interface (≈15 cm depth) (Figure 5a). The volumetric water content below the interface remained 25% higher than that above, indicating localized water accumulation. The contour plots showed a concentration of high-moisture immediately below the geotextile, confirming the onset of a capillary barrier effect (Figure 8a). This was attributed to the relatively large pore openings of Mirafi N140 that prevented upward continuity of water films, creating a localized saturation zone. In the ELD geotextile column, however, the moisture distribution was comparatively uniform (Figure 6a). Both the temporal and contour data showed no abrupt changes across the interface, reflecting effective capillary connectivity maintained by the hydrophilic 4DG fibers. This response demonstrates the lateral redistribution within the wicking fabric that minimized moisture accumulation. This behavior is analogous to the action of capillary-active layers in pavement systems, which regulate suction and control excessive moisture accumulation at the subgrade–subbase interface.

When the water table was raised by 1″, differences in the response among the three configurations became more pronounced. In the control column, the wetting front advanced upward by roughly 25 mm, and equilibrium was re-established within about 1500 min (Figure 4b). The smooth upward progression of contours reflected unimpeded vertical flow, similar to transient water-table rises observed in natural subgrades following intense rainfall (Figure 7b). The soil column with non-woven geotextile, however, exhibited a rapid increase in moisture content below the interface while maintaining near-constant values above it (Figure 5b). This produced a horizontal band of high-moisture content visible in the contours, representing a localized moisture storage beneath the geotextile (Figure 8b). The water storage increased by approximately 6 mm, corresponding to delayed breakthrough across the interface. Such behavior highlights field conditions in pavement sections where non-woven separator geotextiles temporarily trap water during rapid groundwater rise, causing elevated pore pressures and localized reductions in shear strength. The ELD geotextile, in contrast, showed a smaller net increase in storage and reached steady state within 1500 min, which accounts for three times faster than the non-woven system (Figure 6b). The contours advanced upward smoothly without distortion, confirming uniform redistribution of water facilitated by capillary wicking and in-plane drainage (Figure 9b). This lateral redistribution mechanism is similar to that occurring in geosynthetic drainage layers that quickly equilibrate pore-water pressures after rainfall events, thereby reducing differential softening in pavement subgrades.

During the drainage stage, the reservoir was removed to simulate a falling groundwater table, the control column exhibited a uniform and progressive decrease in volumetric moisture content, corresponding to gravity-driven flow typical of drying subgrades under recession conditions (Figure 4c). In the non-woven column, however, drainage was impeded at the interface due to the difference in hydraulic conductivity between the soil and non-woven geotextile, causing water retention above the geotextile and a gradual rate of moisture reduction (Figure 5c). The contours revealed persistent higher moisture zones above the geotextile even after prolonged drainage, illustrating poor desaturation and low drainage efficiency (Figure 8c). Such delayed recovery replicates field conditions where

trapped moisture persists at separator interfaces, preventing the re-establishment of suction and stiffness after wetting. In contrast, the ELD geotextile displayed a rapid and near-uniform decrease in moisture throughout the column (Figure 6c). The contours descended evenly with minimal curvature, demonstrating simultaneous vertical and lateral drainage through the geotextile plane. This accelerated desaturation parallels the field performance of wicking geotextiles that enable faster drying of the pavement base–subgrade system following rainfall or groundwater recession, maintaining the subgrade within an optimal suction range and reducing the duration of low-stiffness conditions.

Under infiltration conditions, when water was introduced from the top at 0.4 mL/min, all columns exhibited a general increase in moisture, but the rate and distribution varied considerably. The control column displayed a gradual increase in moisture at all depths, and the contours showed evenly advancing wetting fronts, consistent with uniform infiltration through a homogeneous soil (Figures 4d and 7d). The non-woven column, however, showed a rapid rise in moisture content near the surface, followed by delayed response at lower sensors, with pronounced contour gradients above the geotextile (Figure 5d). This behavior indicates temporary ponding and slower percolation through the interface. The storage increases and steep gradients above the interface simulate the field response of pavement sections experiencing rainfall infiltration, where non-woven separators restrict downward drainage, leading to short-term moisture accumulation and subgrade weakening. The ELD geotextile displayed a markedly different behavior compared to the non-woven geotextile. Moisture increase was nearly synchronous across all depths, and the contours maintained parallel spacing, signifying uniform infiltration and rapid redistribution (Figures 6d and 9d). A significant effect of ELD geotextiles was noticed around 2 inches of the soil-ELD geotextile interface. The total storage increase was limited, and as much of the infiltrating water was drained laterally along the wicking fibers. This efficient redistribution is similar to the capillary drainage mechanism observed in field pavements with horizontally wicking fabrics, where infiltrated water is quickly diverted toward the pavement edge drains, reducing ponding and moisture-induced degradation.

The combined interpretation of the time-series and contour data highlights the mechanistic distinctions among the three systems. The control column maintained hydraulic continuity dictated solely by the soil–water retention properties of the soil. The non-woven geotextile created a hydraulic discontinuity that restricted vertical flow, leading to excess water storage during wetting and residual moisture during drying. Such conditions would result in transient stiffness loss and increased rutting potential in pavement subgrades due to delayed drainage and localized saturation. The ELD geotextile, on the other hand, maintained hydraulic continuity and enhanced drainage by integrating capillary wicking with in-plane flow, resulting in balanced vertical and lateral flow. Quantitatively, the wicking geotextile reduced total moisture storage by approximately 25–30% and improved drainage efficiency by over 40% relative to the non-woven system. Spatially, the high moisture zone ($\theta > 0.25$) contracted from 14 cm in the non-woven column to 8 cm in the ELD column, while the time to reach quasi-steady conditions decreased from about 7000 min to 2500 min. These improvements correspond to field benefits such as faster drainage recovery, lower pore pressures, and reduced seasonal moisture variation within the subgrade.

The laboratory findings correspond closely with the in situ pavement behavior. Conventional non-woven geotextiles can trap moisture and delay drainage under cyclic wetting, leading to temporary loss of stiffness. In contrast, ELD geotextiles facilitate capillary-driven lateral drainage, rapidly equilibrating porewater pressures and preventing localized water storage. This mechanism maintains uniform moisture and enhances pavement durability under variable hydrological conditions

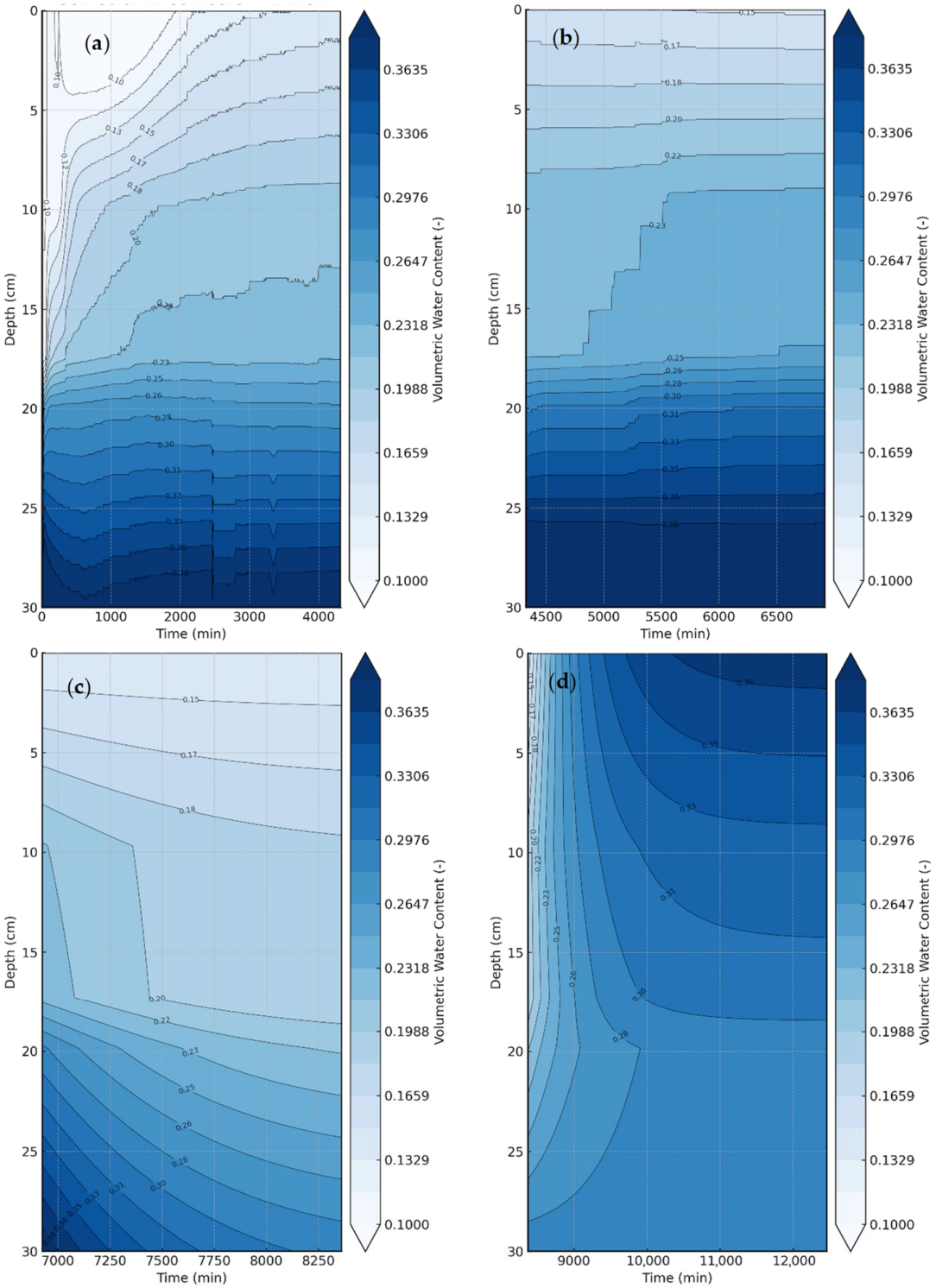

Figure 7. Moisture contour plots with time for the control column along different stages: (**a**) water table at 2″ from base, (**b**) water table at 3″ from base, (**c**) drained condition, (**d**) infiltration at the rate of 0.4 mL/min.

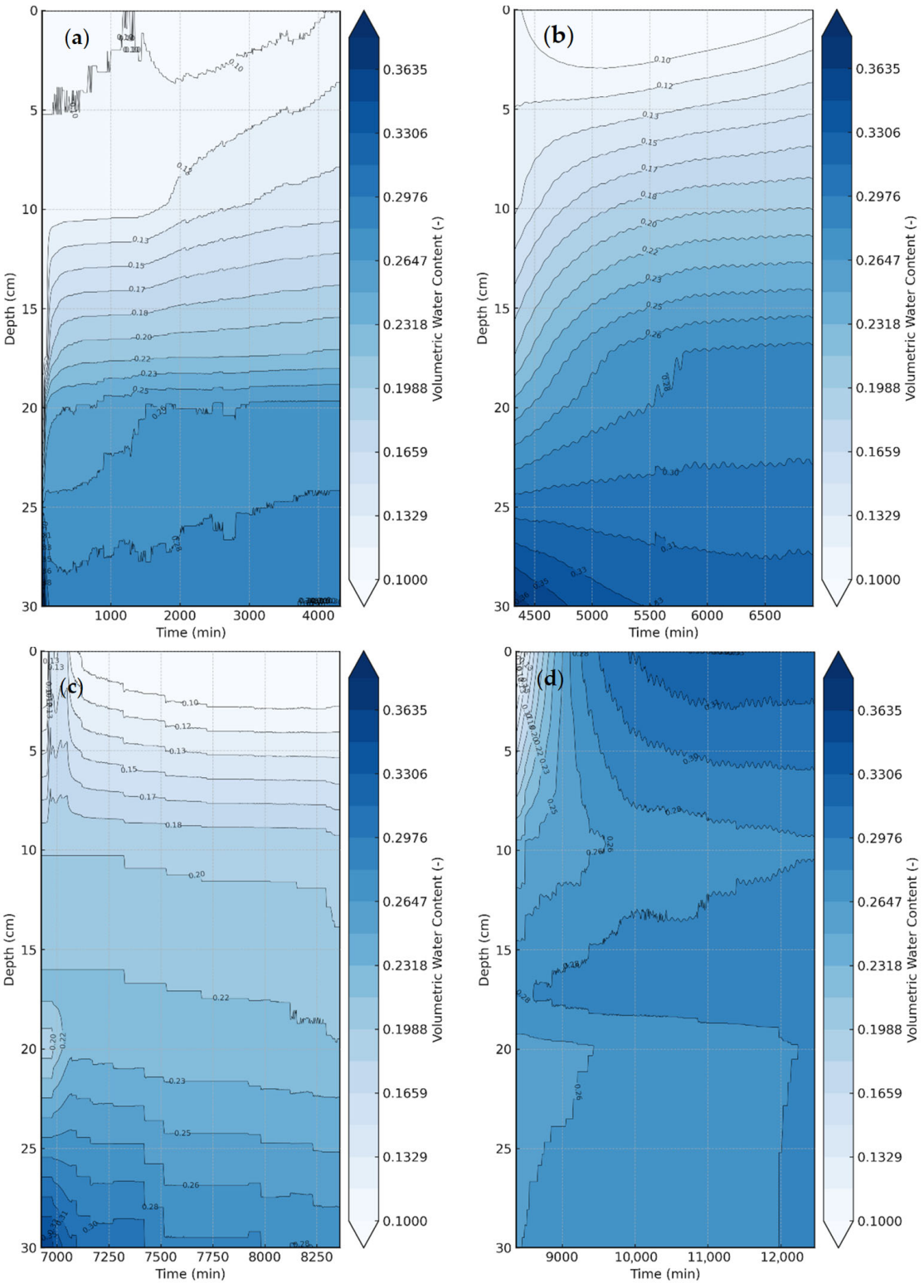

Figure 8. Moisture contour plots with time for the column with a non-woven textile along different stages: (**a**) water table at 2″ from base, (**b**) water table at 3″ from base, (**c**) drained condition, (**d**) infiltration at the rate of 0.4 mL/min.

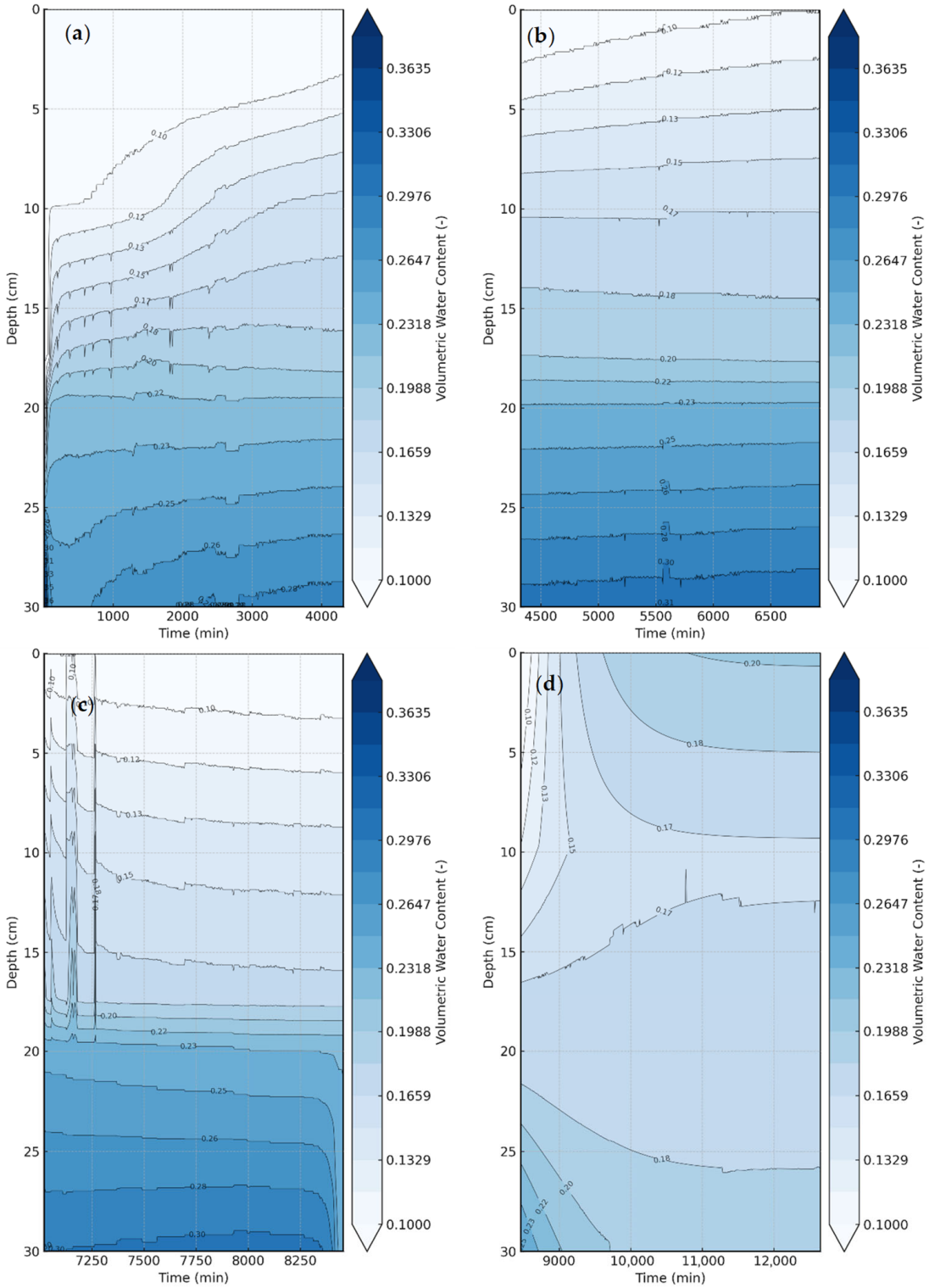

Figure 9. Moisture contour plots with time for the column with an ELD geotextile along different stages: (**a**) water table at 2″ from base, (**b**) water table at 3″ from base, (**c**) drained condition, (**d**) infiltration at the rate of 0.4 mL/min.

3.2. Evolution of Moisture and Suction Profiles with Time

The daily variation of volumetric moisture content and matric suction with depth for the control column, the non-woven geotextile column, and the ELD geotextile column is presented in Figures 10 and 11. These plots provide a day-by-day assessment of how

the soil moisture and suction fields evolved throughout the nine-day testing sequence, comprehending the initial equilibrium, water table rise, drainage, and infiltration stages. The profiles facilitate understanding the redistribution mechanisms occurring within each soil–geotextile system, highlighting the influence of capillary continuity, interfacial flow impedance, and lateral drainage under changing hydraulic boundaries.

At the initial condition, all columns displayed similar moisture and suction distributions, with volumetric water contents ranging from approximately 0.10 near the surface to 0.35 near the base, corresponding to matric suctions of 1800–2500 kPa at the top and near-zero values at the lower boundary (Figures 10a and 11a). Over the first three days, corresponding to the equilibrium and early rise in water table stages, the control column exhibited a uniform upward progression of the wetting front (Figure 10a–e). The increase in volumetric water content with elevation was gradual and proportional, while the suction profiles showed a consistent reduction in suction near the base as the phreatic surface advanced upward (Figure 11a–e). This trend demonstrates continuous hydraulic connectivity, similar to subgrades where shallow groundwater rises or infiltration from adjacent shoulders promotes uniform wetting of the lower layers.

In contrast, the non-woven geotextile column exhibited an early deviation from this behavior. Moisture profiles during Days 1–5 show a distinct inflection near the geotextile level (≈15 cm depth), where water content below the interface increased sharply to about 0.28–0.32, while the layer immediately above remained comparatively dry. The corresponding suction profiles show an abrupt jump at the same location, with suction above the geotextile remaining as high as 800–1000 kPa even after several days. This combination of high suction and low water content above the geotextile indicates the formation of a hydraulic break, resulting from the large pore openings and hydrophobic polymer surfaces of the non-woven fibers. Because the effective radius of the inter fiber pores is relatively large and the contact angle exceeds 90°, the capillary pressure required for upward flow could not be sustained, preventing continuity of the liquid phase. The ELD geotextile column displayed a markedly different evolution during the same period. The suction profiles confirmed a smoother gradient across depth, indicating maintained hydraulic connectivity. This is attributed to the hydrophilic 4DG nylon fibers within the Mirafi H2Ri, which sustain capillary films along their grooved surfaces and promote lateral transmission of water even under low suction gradients. The observed uniformity demonstrates that the wicking geotextile successfully redistributed the upward capillary flux laterally, preventing the formation of localized moisture zones. The 4DG nylon filaments, with deep longitudinal grooves, generate high capillary suction due to their extremely small effective radius and wetting surface ($\theta < 90°$). These grooves rapidly absorb moisture films from adjacent soil pores, maintaining continuous menisci even under low saturation. As the water table was raised by 1″, the capillary fringe advanced upward, increasing the moisture content and lowering the matric suction in the surrounding soil. The increased saturation reduced soil suction to about 750 kPa. As the matric suction recovered quickly after the rise (See Figure 10e), the effective stress in the subgrade remained stable, preventing strength loss typically observed in hydrophobic or non-wicking systems.

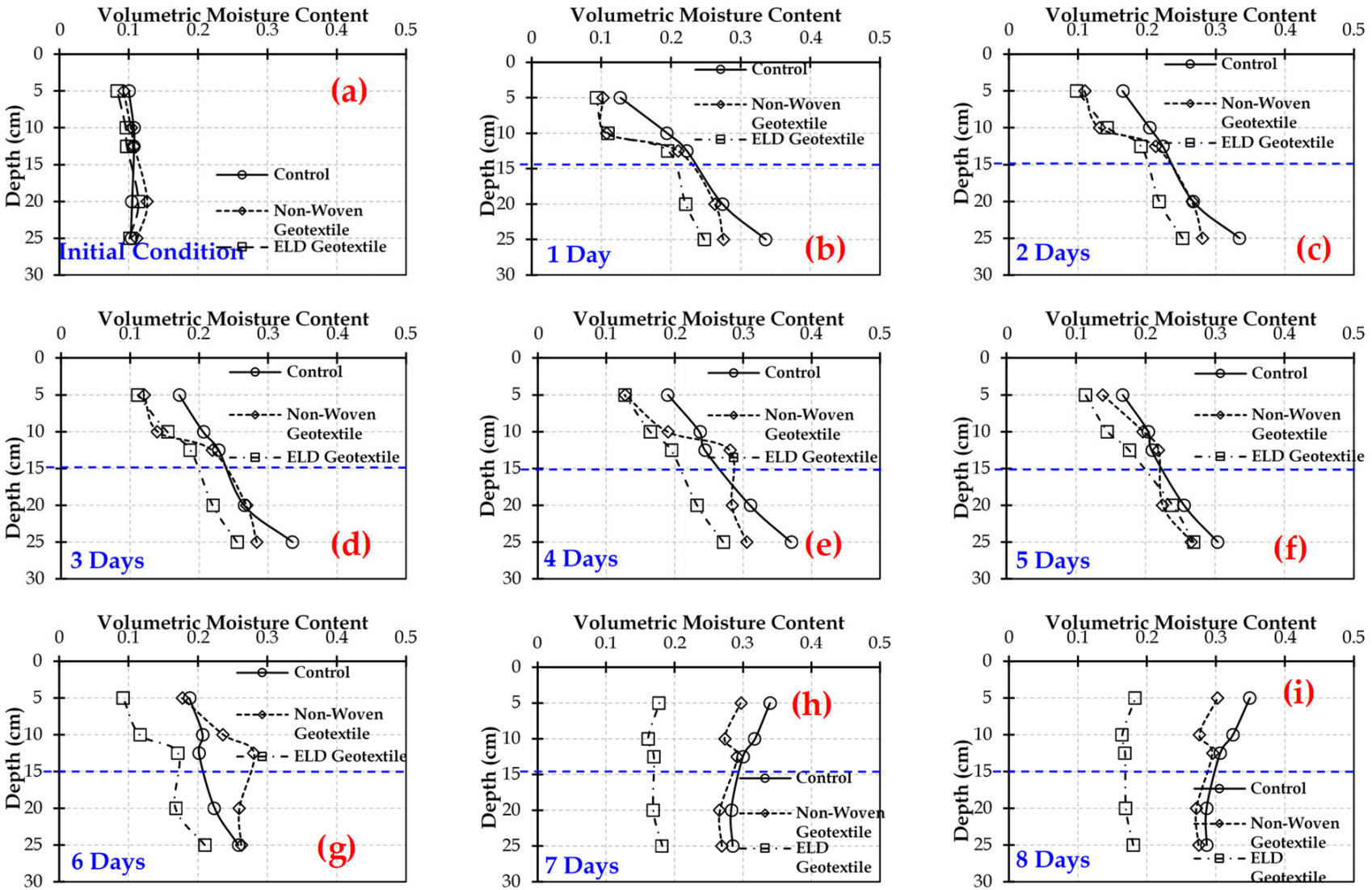

Figure 10. Variation in moisture profiles along depth for different soil columns.

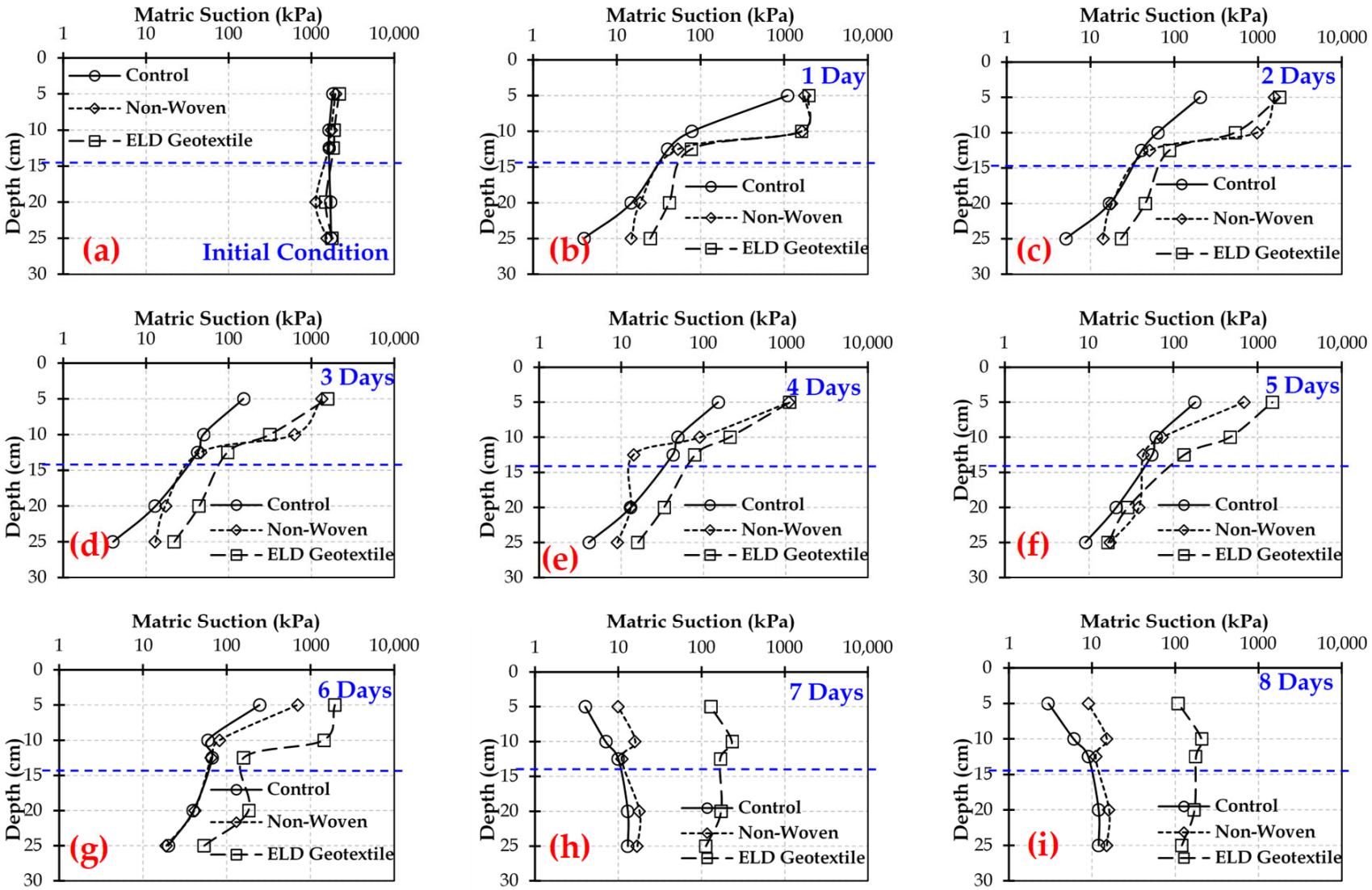

Figure 11. Variation in suction profiles along depth for different soil columns.

By day 6, during the drainage phase, distinct differences in hydraulic response became evident. The control column exhibited a moderate downward shift in the moisture profile, with moisture decreasing by approximately 0.03–0.05 at mid depths and the suction increasing gradually with height as gravitational drainage progressed. The non-woven geotextile column, however, retained high moisture content above the interface ($\theta \approx 0.20$–0.22) with negligible reduction over time, and the suction profiles showed a persistent discontinuity across the interface. The suction below the geotextile increased sharply, indicating air entry and partial desaturation, while the upper zone retained moisture pertaining to boundary effect zone, such conditions are analogous to hydraulic barriers persisting above separator geotextiles in the field during drying cycles. The ELD column, conversely, showed a rapid and uniform decrease in moisture content across depths. The suction gradient remained smooth and continuous, reflecting accelerated drainage through lateral flow paths. The rate of suction recovery in the ELD column was nearly twice that of the control and more than three times that of the non-woven column, confirming its superior drainage efficiency and suction restoration capability. This smooth suction recovery reduced the potential for differential settlement and maintained the soil's structural integrity by preventing rapid collapse of suction and pore pressure imbalances.

During Days 7–8, corresponding to the infiltration stage, the control column showed a steady increase in moisture across depths, indicating typical downward percolation through the soil matrix. The non-woven column again exhibited moisture accumulation in the upper zone ($\theta > 0.35$) with delayed response below the geotextile, while the suction profiles showed a decrease in suction near the surface but minimal change beneath the interface. This behavior demonstrates that the non-woven geotextile restricts downward infiltration, functioning temporarily as a hydraulic impedance layer. In contrast, the ELD geotextile column displayed a uniform moisture profile across all depths and nearly uniform suction reduction, suggesting that infiltrating water was efficiently transmitted laterally along the wicking fibers. Instead of accumulating above the fabric, water was redistributed along the geotextile toward the edges. Because the fabric boundaries were exposed to the atmosphere, a humidity gradient developed between the moist interior and the drier external air, promoting vapor diffusion and gradual drying at the open edges.

The combined evolution of moisture and suction profiles across the testing period reveals clear mechanistic distinctions among the three configurations. The control column maintained consistent capillary continuity, with storage and drainage governed solely by the soil's water retention characteristics. The non-woven geotextile introduced a hydraulic discontinuity, leading to moisture retention above the interface and delayed drainage representing field conditions of transient softening and suction loss often recorded in subgrades incorporating non-woven separators under variable moisture conditions. The ELD geotextile conversely acted as a capillary active drainage layer that redistributed water more efficiently through its hydrophilic fiber network, thereby maintaining near continuous suction gradients and limiting moisture storage. Quantitatively, by the end of the test (Day 9), the mean volumetric moisture content in the upper 10 cm of the non-woven column was approximately 22% higher than the control and 36% higher than the ELD system, while the corresponding mean matric suction in the ELD column was about 1.8 times greater than that in the non-woven column, demonstrating its faster drainage and improved suction recovery.

3.3. Water Storage Behavior of Soil–Geotextile Systems

The variation in water storage above and below the geotextile interface for the non-woven and ELD geotextile columns under different hydraulic boundary conditions is presented in Figure 12. The results provide a quantitative basis for evaluating how each

geotextile influences moisture accumulation, drainage, and redistribution across the soil–geotextile interface. The calculated storage represents the integrated change in volumetric water content over the depth intervals above and below the geotextile during each stage, serving as an indicator of both transient retention and drainage efficiency.

The moisture storage within the soil columns was determined following the formulation proposed by [21], which represents the volumetric integration of water content change over the depth of the profile. For each test stage, the variation in volumetric water content measured by sensors at discrete depths was used to compute the incremental change in storage within each soil layer. The soil column was discretized by interpolating volumetric water content between adjacent sensor depths, and each interpolated interval was assigned a corresponding layer thickness based on the midpoint spacing. The total change in water storage between two-time steps, t_1 and t_2, was calculated as

$$\Delta S = \sum_{i=1}^{n} [\theta_i(t_2) - \theta_i(t_1)] \Delta z_i \quad (1)$$

where, ΔS is the total change in water storage within the soil column (mm of water), $\theta_i(t_1)$ and $\theta_i(t_2)$ is volumetric water content (m^3/m^3) of the i-th layer at times t_1 and t_2, respectively, Δz_i is the thickness of the i-th soil layer or the vertical interval between adjacent sensors (mm), and n is the number of soil layers or measurement intervals considered above and below the geotextile interface.

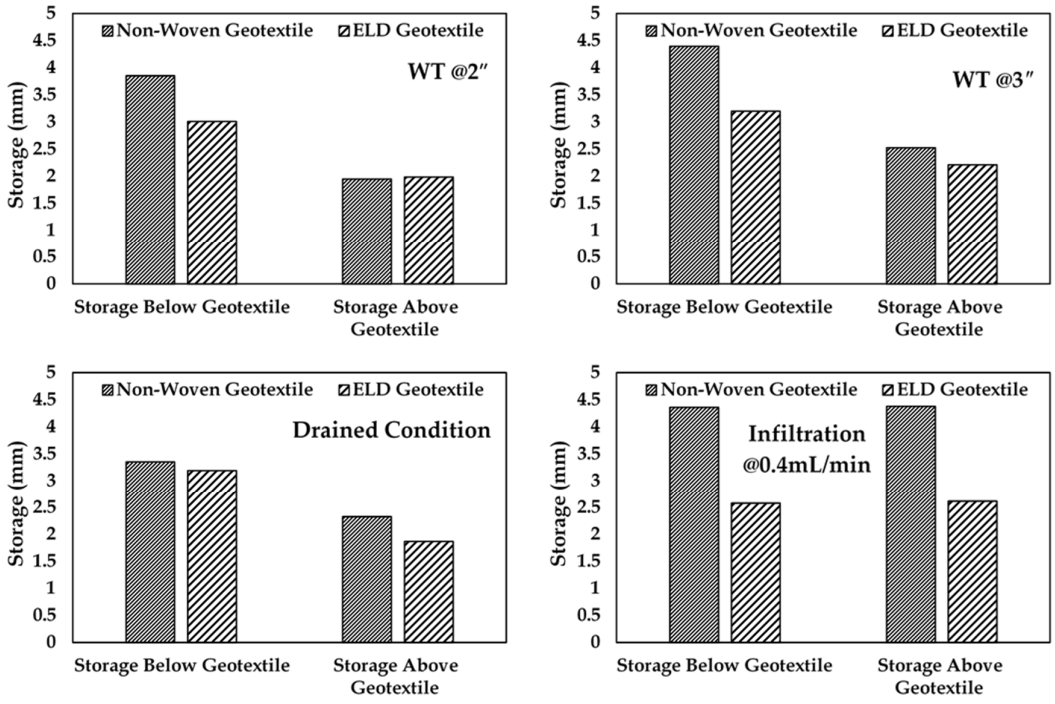

Figure 12. Comparison of moisture storage above and below non-woven and ELD geotextiles at different stages.

The observed water storage patterns clearly illustrate the contrasting hydraulic coupling mechanisms between the soil and each geotextile type. The quantified storage fluctuated between about 4–5 mm below and 2–3 mm above the fabric, forming a cyclic build-up and release pattern typical of a capillary barrier. In the non-woven system, the hydrophobic fibers and large inter fiber pores created a high entry head and a sharp reduction in capillary conductivity at the soil–geotextile interface. This differentiation caused temporary moisture accumulation below the fabric until the local suction decreased enough

to overcome the entry pressure, after which intermittent flow resumed. Such periodic flow produced cyclic variations in storage, reflecting a nonlinear water balance response with pronounced hysteresis during wetting and drying. The interface exhibited a cyclic moisture storage behavior, taking and releasing water as the hydraulic barrier developed and dissipated. Under field conditions, this behavior can lead localized saturation zones that reduces matric suction by 50–70%, and transient subgrade softening or loss of resilient modulus. In contrast, the ELD geotextile maintained nearly constant total storage throughout all stages (≈ 3 mm below and 2–3 mm above). exhibited strong hydraulic continuity and rapid equilibration across the interface. The 4DG fibers retained liquid films within their grooves even under negative pore pressures, ensuring continuous capillary contact with the surrounding soil and preventing air entry. As a result, the fabric acted as an extension of the unsaturated flow domain rather than a barrier, transmitting pressure and moisture changes almost instantaneously along its plane. Consequently, storage variations at the interface remained minimal ($\Delta S \approx$ constant) despite changes in boundary conditions.

Furthermore, the response time was different in both the systems. The non-woven geotextile showed delayed equilibration after boundary shifts, with storage peaks lagging several hours behind imposed conditions, indicative of low interfacial diffusivity. Conversely, the ELD system responded within minutes, signifying higher flow and nearly instantaneous suction propagation. Hydromechanically, the ELD layer functioned as a capillary damping medium that moderated pore-pressure fluctuations and stabilized suction in the adjacent soil. This behavior is especially beneficial under cyclic infiltration or fluctuating groundwater levels, preventing repeated suction collapse and the associated reductions in small strain stiffness. The persistence of liquid films within the 4DG fiber grooves and inter yarn spaces preserves capillary continuity across contrasting materials, similar to the bridging behavior of menisci between soil particles during desaturation. Thus, the soil–geotextile composite acts as a single hydraulic continuum with smooth suction transitions rather than discrete zones separated by a hydraulic break. This integrated response reduces transient storage, limits hysteresis in the soil–water characteristic curve, and facilitates faster suction recovery after infiltration. These combined mechanisms emphasize superior ability of the ELD geotextile to stabilize moisture conditions and preserve the mechanical performance of pavement subgrades under variable climate and loading cycles.

4. Conclusions

A systematic experimental program was conducted to investigate the transient hydraulic behavior of soil columns incorporating non-woven and enhanced lateral drainage (ELD) geotextiles simulating realistic field boundary conditions, including steady groundwater equilibrium, rising water table, drainage, and surface infiltration, to capture the full range of hydrological scenarios typically experienced by pavement subgrades. Continuous measurements of volumetric moisture content and matric suction were used to quantify changes in water storage, suction recovery, and moisture redistribution across the soil–geotextile interface. The tests were designed not only to compare the hydraulic response of two contrasting geotextiles but also to elucidate the underlying capillary and wicking mechanisms governing unsaturated flow within their pore structures. The major findings and engineering implications are summarized as follows:

1. The control column exhibited continuous capillary rise and uniform wetting–drying behavior governed solely by the soil's water retention properties. Introducing a non-woven geotextile disrupted this continuity, creating a hydraulic discontinuity at the interface that caused localized moisture accumulation and delayed suction recovery. In contrast, the ELD geotextile maintained capillary connectivity through

its hydrophilic 4DG fibers, enabling lateral redistribution of water and maintaining a smooth suction transition across the interface.

2. During groundwater rise and surface infiltration, the non-woven geotextile acted as a temporary hydraulic barrier, increasing total storage by 25–30% relative to the control column and delaying equilibrium. The ELD geotextile exhibited self-regulating drainage, maintaining nearly constant storage as inflow was balanced by lateral outflow and partial vapor dissipation through open edges. This equilibrium response represents a quasi-steady state condition typical of field pavements where wicking fabrics prevent excessive pore water buildup during short term wetting events.
3. The ELD geotextile demonstrated a drainage efficiency nearly double that of the non-woven fabric. The suction profiles showed faster desaturation and smoother recovery gradients, indicating that the 4DG fibers retained hydraulic connectivity even under high suctions. The enhanced suction recovery contributes directly to higher shear strength and resilient stiffness of the subgrade under cyclic moisture variation.
4. The contour plots revealed that the ELD geotextile maintained a stable and continuous moisture field, reducing the vertical extent of the high moisture zone by nearly 40% compared with the non-woven system. Our results show that the ELD geotextile facilitated efficient lateral drainage, with a consistent influence zone extending up to 2 inches below the fabric. This improved uniformity reflects the effective integration of capillary wicking and in-plane flow, which prevents localized saturation above the interface.
5. The laboratory findings directly translate to field conditions in pavement subgrades exposed to seasonal fluctuations in groundwater and rainfall. Non-woven geotextiles, while effective as separators, can trap water and induce transient loss of stiffness. Conversely, ELD geotextiles mitigate moisture buildup through capillary-driven lateral drainage, maintaining consistent suction and improving the hydraulic resilience of pavement systems.

However, the findings presented in this study are based on tests conducted on a single soil mixture using a one-dimensional column configuration. While the results provide mechanistic insight into the unsaturated hydraulic behavior of ELD geotextiles, further investigation across different soil types, stress conditions, and two dimensional or three-dimensional boundary configurations is required before broad field application can be fully established.

Author Contributions: S.A.M.: Conceptualization, Methodology, Investigation, Data curation, Formal analysis, writing—original draft, Writing—review and editing. J.G.Z.: Funding Acquisition, Conceptualization, Methodology, Visualization, Writing—review and editing, Supervision. All authors have read and agreed to the published version of the manuscript.

Funding: The authors gratefully acknowledge the financial and material support provided by Solmax for this research. The views and conclusions expressed in this paper are those of the authors and do not necessarily reflect the views of the sponsor.

Data Availability Statement: The raw data supporting the conclusions of this article will be made available by the authors upon request.

Conflicts of Interest: The authors declare that they have no known competing financial interests or personal relationships that could have appeared to have influenced the work reported in this paper.

References

1. Fredlund, D.G.; Rahardjo, H. *Soil Mechanics for Unsaturated Soils*; Wiley: New York, NY, USA, 1993.
2. Lu, N.; Likos, W.J. *Unsaturated Soil Mechanics*; Wiley: New York, NY, USA, 2004.

3. Rahardjo, H.; Lim, T.T.; Chang, M.F.; Fredlund, D.G. Shear-strength characteristics of a residual soil under drying and wetting. *J. Geotech. Geoenviron. Eng.* **2004**, *130*, 879–889.
4. Cuelho, E.V.; Perkins, S.W.; Morris, Z. Moisture effects on geosynthetic-reinforced pavement performance. *Transp. Res. Rec.* **2014**, *2404*, 33–43.
5. Han, J.; Zhang, Y. Mechanistic evaluation of moisture variation in pavement subgrades. *J. Transp. Eng. Part B Pavements* **2020**, *146*, 04020022.
6. Khire, M.V.; Benson, C.H.; Bosscher, P.J. Field data from a capillary barrier and model predictions with UNSAT-H. *Water Resour. Res.* **1999**, *35*, 3149–3165. [CrossRef]
7. Korkiala-Tanttu, L. Moisture sensitivity of base materials in pavements. *Road Mater. Pavement Des.* **2012**, *13*, 555–569.
8. Erlingsson, S.; Rahman, M.S. Moisture impact on mechanical behavior of unbound granular materials. *Road Mater. Pavement Des.* **2015**, *16*, 245–260.
9. Puppala, A.J.; Hoyos, L.R.; Nazarian, S. Moisture sensitivity of unbound pavement layers. *Transp. Geotech.* **2018**, *17*, 58–68.
10. Konrad, J.M.; Morgenstern, N.R. Frost heave in soils. *Can. Geotech. J.* **1980**, *17*, 473–486. [CrossRef]
11. Puppala, A.J.; Nazarian, S. Moisture effects on subgrade stiffness. *Transp. Res. Rec.* **2021**, *2675*, 350–364.
12. Han, J.; Lin, H.; Zhang, Y. Climate-adaptive drainage design using wicking geotextiles. *Transp. Geotech.* **2022**, *34*, 100771.
13. Zhang, X.; Lu, D.; Han, J. Influence of moisture variation on resilient behavior of fine-grained subgrades. *Transp. Geotech.* **2017**, *13*, 85–95.
14. Rathod, D.; Abid, M.S.; Vanapalli, S.K. Performance of polypropylene textile encased stone columns. *Geotext. Geomembr.* **2021**, *49*, 222–242. [CrossRef]
15. Giroud, J.P.; Han, J. Design method for geogrid-reinforced unpaved roads. *J. Geotech. Geoenviron. Eng.* **2004**, *130*, 775–786. [CrossRef]
16. Koerner, R.M. *Designing with Geosynthetics*, 6th ed.; Xlibris: Philadelphia, PA, USA, 2012.
17. Abid, M.S.; Rathod, D.; Vanapalli, S.K. Experimental and numerical studies on geosynthetic encased stone columns in saturated and unsaturated soils. *Transp. Geotech.* **2025**, *52*, 101566. [CrossRef]
18. Christopher, B.R.; Perkins, S.W.; Holtz, R.D. *Geosynthetic Design and Construction Guidelines (FHWA-NHI-07-092)*; Federal Highway Administration (FHWA): Washington, DC, USA, 2010.
19. Perkins, S.W. *Mechanistic–Empirical Design of Geosynthetic-Reinforced Flexible Pavements*; NCHRP Report; Transportation Research Board: Washington, DC, USA, 2011; p. 512.
20. McCartney, J.S.; Zornberg, J.G. Evaluation of drainage in geosynthetic capillary barrier systems. *Geotext. Geomembr.* **2008**, *26*, 356–368.
21. Stormont, J.C.; Morris, C.E. Method to estimate water-storage capacity of capillary barriers. *J. Geotech. Geoenviron. Eng.* **1998**, *124*, 297–302. [CrossRef]
22. Fredlund, D.G.; Rahardjo, H.; Fredlund, M.D. *Unsaturated Soil Mechanics in Engineering Practice*; Wiley: Hoboken, NJ, USA, 2012.
23. Ross, B. The diversion capacity of capillary barriers. *Water Resour. Res.* **1990**, *26*, 2625–2629. [CrossRef]
24. Stormont, J.C.; Anderson, C.E. Capillary barrier performance in field tests. *J. Geotech. Geoenviron. Eng.* **1999**, *125*, 783–794.
25. Touma, J.; Vauclin, M. Experimental and numerical analysis of two-phase flow through unsaturated soil. *Water Resour. Res.* **1986**, *22*, 729–738.
26. Zornberg, J.G. Geosynthetic capillary barriers: Current state of knowledge. *Geosynth. Int.* **2010**, *17*, 273–300. [CrossRef]
27. Zornberg, J.G.; Bouazza, A.; McCartney, J.S. Geosynthetic capillary barriers: Principles and applications. *Geotext. Geomembr.* **2009**, *27*, 1–8.
28. Morris, C.E.; Stormont, J.C. Capillary barriers and water balance in cover systems. *J. Geotech. Geoenviron. Eng.* **1997**, *123*, 543–553.
29. Aubertin, M.; Mbonimpa, M.; Bussière, B.; Chapuis, R.P. A model to predict water flux through unsaturated waste rock piles. *Can. Geotech. J.* **1999**, *36*, 55–69.
30. Benson, C.H.; Albright, W.H.; Apiwantragoon, P. Field evaluation of capillary barriers for cover systems. *J. Geotech. Geoenviron. Eng.* **2011**, *137*, 1079–1093.
31. Gallage, C.P.K.; Uchimura, T. Effects of capillary barriers on rainfall infiltration in slopes. *Soils Found* **2010**, *50*, 949–960.
32. Rahardjo, H.; Ong, T.H.; Rezaur, R.B. Infiltration and stability of soil slopes with capillary barriers. *Soils Found.* **2012**, *52*, 208–220.
33. Azevedo, M.; Zornberg, J.G. February. Capillary barrier dissipation by new wicking geotextile. In Proceedings of the Panamerican Conference on Unsaturated Soils, Cartagena, Colombia, 20–22 February 2013; pp. 20–22.
34. Azevedo, M.; Zornberg, J.G. Geotechnical problems and soil atmosphere interaction Capillary barrier dissipation by new wicking geotextile. In *Advances in Unsaturated Soils*; CRC Press: Boca Raton, FL, USA, 2013; pp. 577–584.
35. Chen, Y.; Han, J.; Lin, H. Performance of wicking geotextiles for drainage improvement under unsaturated conditions. *Geotext. Geomembr.* **2023**, *51*, 1–12.
36. El Hachem, A. Enhanced lateral drainage geotextile to mitigate the detrimental effects of moisture in pavements. In Proceedings of the Geo-Congress 2019, Philadelphia, PA, USA, 24–27 March 2019; pp. 225–235.

37. Han, J.; Lin, H. Evaluation of wicking geotextiles for pavement drainage. *J. Geotech. Geoenviron. Eng.* **2019**, *145*, 04019105.
38. Lin, H.; Han, J.; Chen, Y. Quantifying and incorporating the benefits of wicking geotextiles into pavement design. *J. Transp. Eng. Part B Pavements* **2021**, *147*, 04021006. [CrossRef]
39. Azevedo, A.M.M. Hydraulic Performance of Wicking Geotextiles under Unsaturated Conditions. Ph.D. Dissertation, The University of Texas at Austin, Austin, TX, USA, 2016.
40. Zornberg, J.G.; Odgers, B.; Roodi, G.H.; Azevedo, M.M. Advantages and applications of enhanced lateral drainage in pavement systems. *Proc. GeoAfrica* **2013**, 539–548.
41. Zornberg, J.G.; Azevedo, M.; Sikkema, M.; Odgers, B. Geosynthetics with enhanced lateral drainage capabilities in roadway systems. *Transp. Geotech.* **2017**, *12*, 85–100. [CrossRef]
42. Jiang, Y.; Ma, C.; Han, J. Numerical simulation of moisture redistribution in wicking geotextile systems. *Comput. Geotech.* **2023**, *159*, 105244.
43. Orellana-Palomino, J. Hydraulic Behavior of Capillary Barriers and Geosynthetics in Unsaturated Soils. Master's Thesis, The University of Texas at Austin, Austin, TX, USA, 2021.
44. Sicha, G. Hydraulic Performance of Unsaturated Geotextile Interfaces. Ph.D. Dissertation, The University of Texas at Austin, Austin, TX, USA, 2022.
45. AASHTO. *AASHTO Guide for Design of Pavement Structures*; American Association of State Highway and Transportation Officials (AASHTO): Washington, DC, USA, 1993.
46. MEPDG. *Mechanistic-Empirical Pavement Design Guide: A Manual of Practice*; AASHTO: Washington, DC, USA, 2008.
47. Van Genuchten, M.T. A closed-form equation for predicting the hydraulic conductivity of unsaturated soils. *Soil Sci. Soc. Am. J.* **1980**, *44*, 892–898. [CrossRef]
48. Durner, W. Hydraulic conductivity estimation for soils with heterogeneous pore structure. *Water Resour. Res.* **1994**, *30*, 211–223. [CrossRef]